Enhanced Wide-band Infrared Absorptivity of Black Silicon

Sreyash SARKAR[1*], Ahmed A. ELSAYED[1,2], Frédéric MARTY[1], Jérémie DRÉVILLON[3], Yasser M. SABRY[2], Jiancun ZHAO[4], Yiting YU[4], Elodie RICHALOT[1], Philippe BASSET[1], Tarik BOUROUINA[1], and Elyes NEFZAOUI[1]

[1]Université Paris-Est, ESYCOM (FRE2028), CNAM, CNRS, ESIEE Paris, Université Paris-Est Marne-la-Vallée, F-77454 Marne-la-Vallée, France
[2]Electronics and Electrical Com. Depart., Faculty of Eng., Ain Shams University, Cairo, Egypt
[3]Institut Pprime, CNRS, Université de Poitiers, ISAE-ENSMA, Futuroscope Chasseneuil, France
[4]Northwestern Polytechnical University, Xi'an, China
[*](Corresponding author: sreyash.sarkar@esiee.fr)

Abstract –In the present work, we report, on the exceptionally high absorptivity of Black Silicon (BSi) in the spectral range of thermal radiation, which can be instrumental for various thermal radiation related applications. Having fabricated two wafers of BSi having n-type low and high doping, we have found experimentally that for highly doped BSi, a high absorptivity is observed till 15 µm which has also been compared with similarly doped Flat Si (FSi) samples. However, beyond 15 µm, the absorptivity of highly doped BSi sample decreases. Subsequent processing of SEM images reveals that these noteworthy radiative properties can probably be attributed to particular morphological features of heavily doped BSi at the nanoscale. These features are quantified through statistical image processing. Reported results pave the way to highly integrated and effective infrared sources using Black Silicon.

Keywords: absorptivity; black silicon; radiative infrared properties; doping; nanostructures

Nomenclature

N	doping level, cm^{-3}	e	charge of electron, coulomb
ε_∞	high frequency asymptotic value	µ	carrier mobility, $cm^2/(V \cdot s)$
γ	scattering rate for carriers, eV	m^*	carrier effective mass, kg
ωp	plasma frequency of material, radian	m	carrier mass, kg
ω	angular frequency, radian	ε_0	permittivity of free space, F/m
c	speed of light in vacuum, m/s	σ	electrical conductivity, S/m

1. Introduction

Infrared radiative properties of materials are of indispensable significance for several applications involving thermal radiation conversion and management such as sensors [1], thermal rectification [2], perfect absorbers [3,4] radiative cooling [5,6] etc., subsequently, attracting an increased attention in recent years [6]. In the present work, we report, on the properties of Black Silicon (BSi) [4] in the spectral range of thermal radiation, up to 25 µm which can be instrumental for heat transfer applications. BSi has become nowadays, a well-established micro-nano-structured silicon surface [7] that can be obtained by different techniques including cryogenic plasma [6] as considered in this work. BSi exhibits fascinating wetting and optical properties. In particular, due to its specific morphology, it is well-known for its excellent absorption of almost 100% of incident light [7-9], hence its name is *Black* according to its colour to the naked eye [9]. But very little is known about its infrared radiative properties and the possible ways of enhancing them for specific applications. It has been noted since [10,11] that such nano-scale features lead to a critical improvement of silicon absorptivity in the visible range [12]. Having previously shown [13,14] that we can extend such outstanding

https://doi.org/10.25855/SFT2020-067

properties to the mid-infrared (MIR) by using highly doped silicon, in this work we report that the high absorptivity in fact further hinges on to the far-infrared (FIR) range. However, beyond 15 μm, the absorptivity of highly doped BSi sample decreases. We observe that the density of nanostructures on BSi increases with a high level of doping which leads to the increase of absorptivity over an extended spectral range. We show through electromagnetic simulations along with measurements on flat silicon (FSi), the obvious effect of doping on silicon and then proceed towards an experimental on highly doped BSi. We observe that for highly doped BSi, high absorptivity is observed till a wavelength of 15 μm. Subsequent processing of SEM images reveals that these conspicuous radiative properties are presumably due to very specific morphological features of heavily doped BSi at the nanoscale. These features are quantified through statistical image processing. The promulgated outcomes, therefore, prepare the way to highly integrated infrared sources and promising performances in thermal management applications such as passive radiative cooling [15].

2. Methodology

2.1. Material Properties

In the infrared region, the Drude model [16-18] describes the frequency-dependent dielectric function as follows:

$$\varepsilon(\omega) = (n + i\kappa)^2 = \varepsilon_{\infty} - \frac{\omega_p^2}{\omega(\omega + i\gamma)} \quad (1)$$

$$\omega_p = \sqrt{Ne^2/m^*\varepsilon_0} \quad (2)$$

$$\gamma = e/m^*\mu \quad (3)$$

$$m^* = xm \quad (4)$$

where, N is the doping level; $\varepsilon(\omega)$ is the dielectric function; ε_{∞} is the high-frequency asymptotic value that is approximately 11.7 for silicon and is independent of the doping concentration; γ is the scattering rate for carriers in the semiconductor; ω_p is the plasma frequency of the doped material ; $\omega = 2\pi c/\lambda$ is the angular frequency, with c and λ being the speed of light and wavelength in vacuum; e = charge of electron; μ is the carrier mobility; m^* is the carrier effective mass, m is the mass of carrier; ε_0 is the permittivity of free space and $x = 0.27$ or 0.37 for n and p-type respectively. Here, the n-type and p-type are referred to silicon implanted with phosphorus and boron, respectively. Although, the degree of carrier ionization depends on temperature and carrier concentration, both phosphorous and boron dopants are fully ionized at room temperature for the specified range of doping concentrations. The above model has been used popularly in literature in[18] and Basu et. al [17] experimentally validated the model. Using the optical constants, the absorptance of plain silicon can be calculated with the complex Fresnel coefficients.

The spectral absorptance [17] of plain silicon in air at normal incidence can be expressed as:

$$\alpha = \frac{4n_{si}}{(n_{si} + 1)^2 + {\kappa_{si}}^2} \quad (5)$$

However, in recent times, more advanced models have been proposed such as in the work of Law et. al [19] and Cleary et. al [20] adherent to the localized surface plasmon resonances (LSPRs). However, the mid-IR does offer significant flexibility for the plasmonics researcher willing to look past traditional plasmonic materials. In particular, highly doped semiconductors offer a potential replacement for noble metals at long wavelengths. The optical response of a

doped semiconductor can be modelled using the Drude formalism with the separation of the real and the imaginary part of the relative permittivity:

$$\varepsilon(\omega) = \varepsilon_\infty(1 - \frac{\omega_p^2}{\omega^2 + i\omega\gamma}) \quad (6)$$

$$\varepsilon(\omega) = \varepsilon' + i\varepsilon'' = \varepsilon_\infty\left(1 - \frac{\omega_p^2}{\omega^2+\gamma^2}\right) + i\varepsilon_\infty(\frac{\gamma\omega_p^2/\omega}{\omega^2+\gamma^2}) \quad (7)$$

$$\varepsilon(\omega) = \varepsilon' + i\varepsilon'' = \varepsilon' + i\frac{\sigma}{\omega\varepsilon_0} \quad (8)$$

where, σ is the electrical conductivity of the material, which can therefore be expressed, after combining (7) and (8), as:

$$\sigma = \frac{\varepsilon_0\varepsilon_\infty\gamma\omega_p^2}{\omega^2+\gamma^2} \quad (9)$$

2.2. Numerical Methods

In the infrared region, the specific Drude model [16], which describes the frequency-dependent dielectric function of silicon, has been employed with more advanced models [19,20]. Thus, in the various modelling techniques involved in this work such as FEM (Finite Element Mesh Analysis) [21,22] primarily employed for BSi simulations, Rigorous Wave Coupled Analysis (RCWA) [23] for FSi simulations, the equations of Drude formalism [Eqns. 1-9] have been employed to construct the representative models for simulations.

2.2.1. Boundary Conditions

Reflectance simulations by FEM in the infrared wavelength range are performed using ANSYS HFSS software [24]. The silicon model we implemented in HFSS makes use of (Eqns. 1-9) especially the expression for electrical conductivity (Eqn. 9) as inputs to simulate radiative optical properties of highly doped FSi. The source consists in a plane wave with incidence angles of 30˚ and 60˚. At the bottom of the simulated volume, an impedance condition is used to simulate the thickness of the silicon substrate of 500 μm and a perfect conductor is placed under the silicon layer to further match the conditions of the reflectance measurement setup. Simulations are performed by illuminating the studied structure by Transverse Electric (TE)- and Transverse Magnetic (TM)-plane waves and the total reflectance is calculated by averaging both cases and accounting for depolarization effects.

2.3. Experimental Setup for Measurements of Reflectance

Experimental measurements of specular reflectivity have been performed on fabricated samples of two wafers of BSi having n-type doping of 2×10^{18} cm^{-3} (low doping) and 4.5×10^{19} cm^{-3} (high doping). Experimental measurements of specular reflectivity have been performed using a Perkin Elmer Spectrum GX FTIR Spectrometer [25, 26] in a spectral range from 1 to 25 μm at room temperature and at angles of incidences of 30˚ and 60˚. The aforesaid spectrometer has a resolution range of 0.2 to 64 cm^{-1} and a sample area of 1 cm^{-2} detectable by the spectrometer [25]. For mid-infrared, the Mercury Cadmium Telluride (MCT) detector with Potassium Bromide (KBr) window used in the spectrometer has a signal-to-noise ratio of

45000:1. Reflectance measurements on FSi with low and high doping have also been performed for comparison.

2.4. Black Silicon Fabrication

A couple of approaches have been made to restrain the reflectance of silicon by finishing the surface [27-29]. The frameworks of nano-structuration on silicon by reactive ion etching (RIE) [30] and and inductively coupled plasma-reactive ion etching (ICP-RIE), generally deep reactive ion etching (DRIE) [31, 32] have been represented widely in literature. Plasma etching utilizing DRIE is a most likely comprehended technique to gain black silicon surfaces of low reflectance. The DRIE relies upon inductively coupled plasma (ICP) of sulfur hexafluoride (SF6) and licenses anisotropic etching of silicon and this strategy is truly fundamental, quick, and controllable. While the implied 'Bosch' method is the most ordinarily utilized method in DRIE prevalently[31], we have used the cryogenic technique to acquire black silicon surfaces, in this work because although in the DRIE-Bosch technique, the possibility to adjust the duration of the time steps provides greater control on the anisotropic etching profile, the discontinuity between passivation and etching steps may result in a scalloping effect in vertical walls[7]. The fixed parameters for all models are ICP force of 1000 W, gas weight of 1.5 Pa, and SF6 gas stream pressure of 200 sccm[4]. The samples were conveyed on single side cleaned (100)- situated single crystalline silicon wafers of 4 in. breadth, having n-type low doping comparing to a doping level of 2×10^{18} cm^{-3} and for high doping, a doping level of 4.5×10^{19} cm^{-3}, is considered on which a few square samples of 1 cm^2 have been readied.

2.5. Statistics Generation from SEM Images

SEM grey-scale analysis is a reconstruction technique from which a three-dimensional model that represents the surface topography of BSi samples can be obtained. This method consists of inferring the structures' height based on the grey-scale level of a top-view SEM image, using the known height values of the SEM brightest and darkest grey-level as bounds of an interpolating range. While other non-destructive methods of reconstruction such as the ones based on multiple images taken at different viewing angles have been demonstrated, they require repositioning the sample at different viewing angles and robust algorithms to detect the same features in the different images [33]. SEM grey-scale analysis has been effectively used in the reconstruction of BSi samples [34]; however, there are some limitations of the maximum hole depth detectable that are due to the limited SEM dynamical range which is limited to ~20 μm [34]. Therefore, while the SEM grey-scale analysis provides accurate topography information [7,8], it is limited to BSi samples with small or medium aspect ratios. In this work, from top- and side-view SEM pictures, the mean values of periodicity and height of the BSi structures have been extracted by grey-level analysis [34]: all the centers of holes have been identified and each pixel corresponds to a height.

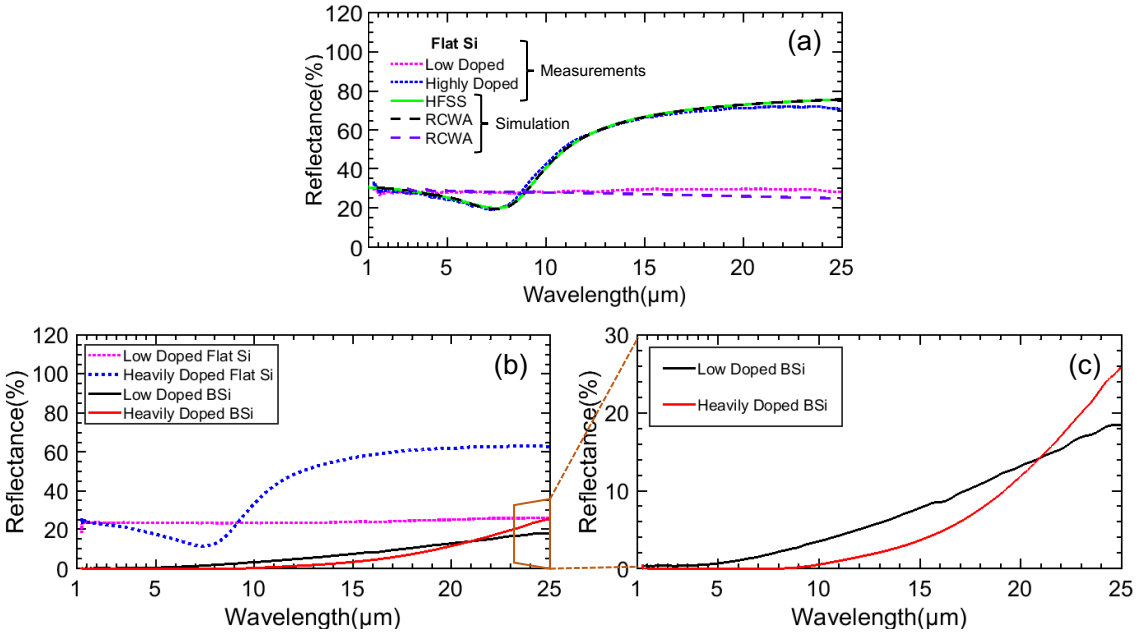

Figure 1: *(a) Comparison of measurements & simulations of specular spectral reflectance of low doped and highly n-doped flat silicon wafers at 60˚angle of incidence (b)Measurements of reflectance on two BSi samples having low and high doping at 30˚angle of incidence compared with FSi. (c) Zoom on the performance of highly doped and low doped BSi.*

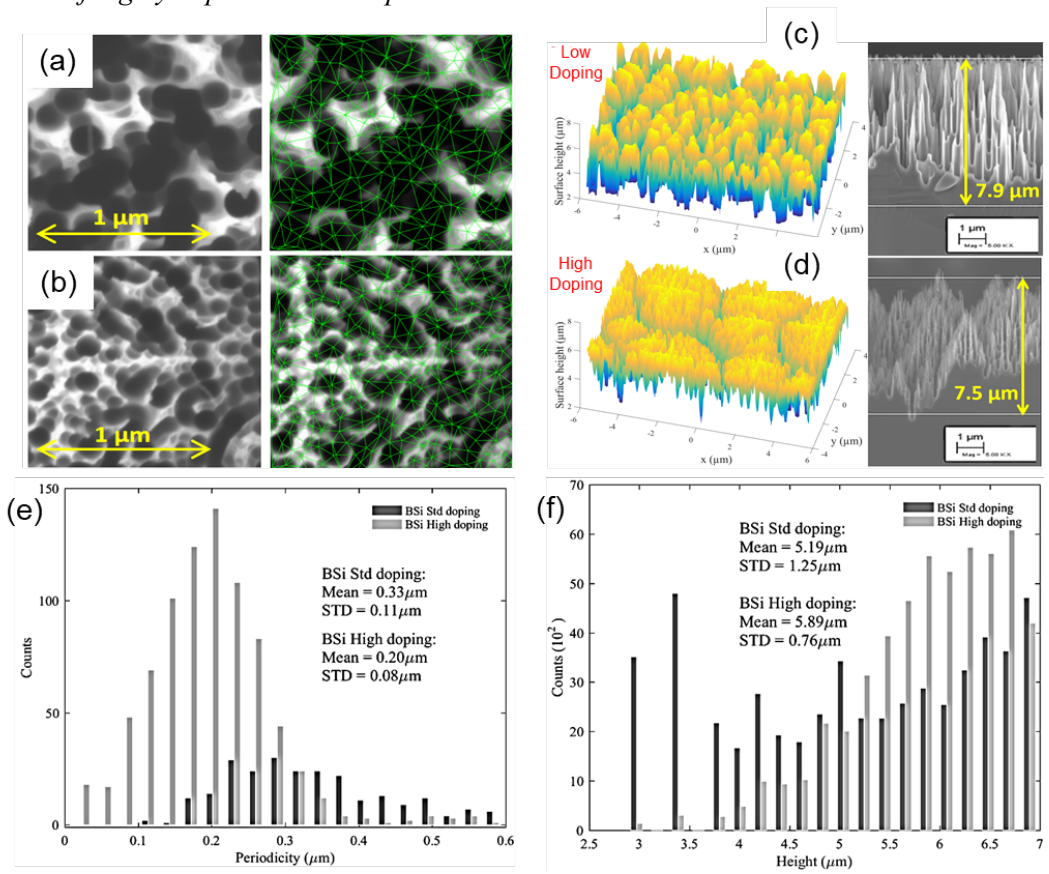

Figure 2: *Morphological analysis of 1.3x1.3 μm² BSi samples obtained from top-view SEM images. (a) SEM and model images of BSi etched on low doped substrate. (b) SEM and model images of BSi etched on a highly doped substrate. 3D reconstruction using gray-level technique from SEM images and side-view SEM for (c) low and (d)highly doped silicon for a similar etching process (e) Histogram of etched hole's periodicity and (f) histogram of structure's height for both samples.*

3. Results

Figure 1 shows the pathway from FSi to BSi, whilst highlighting the near perfect concurrence of spectral measurements with various simulation models employed for FSi, thus validating the numerical models. Figure 1(a) illustrates the specular reflectance responses of two FSi samples along with their agreement with RCWA and FEM simulation models at 60° angle of incidence. We show reflectance results for this particular angle of incidence as it gives us a more concurrence compared to 30°. Figure 1(b) shows the spectral responses of two BSi samples of high and low doping compared with corresponding FSi samples at 30° angle of incidence. Figure 1(c) shows the zooming in on the performance of doped and low-doped BSi. The effects of high doping on the reflectance and on the BSi geometrical features at the nanoscale, can be obviously noted, where, for the highly doped BSi sample, the reflectance is kept lower than the low-doped sample till 21 µm. These particular angles of incidences have been chosen due to the constraints of the measurement setup used.

As a reminder, this figure also recalls the typical responses recorded in the visible range [13]; as most of the time, such a curve shows an increase of reflectance at the highest wavelengths, which also suggests that absorption, should deteriorate if we increase the wavelength further. But surprisingly, this does not happen in our results shown in Figure 1. On the contrary, one can see that reflectance of highly doped BSi sample is kept very low, below 1% up to 10 µm. The reflectance remains even below 0.1% up to 7.5 µm and then starts increasing up to 4% at 15 µm.

At around 21 µm, a crossover happens, where the spectral response of the highly doped sample rises above 15% to reach a maximum of 26% at 25 µm. This however highlights the fact that there is, in all obviousness, a compromise involved. To reach almost 100% light absorption, the highly doped BSi sample is a perfect candidate until 15 µm, but to attempt a broader but lesser absorption, the low doped sample would be ideal. Indeed, considering the spectral distribution of the blackbody intensity given by Planck's function [35] and the fraction emitted in the spectral range covered by our experimental results between 1 and 25 µm, one can note that this fraction reaches 83% and 97 % for a radiation source at 300 K and 600 K, respectively [36]. Such small reflectance, thus high emissivity, in this specific wavelength range is of paramount importance for various applications. Actually, because of the large density of free carriers, heavily doped silicon is opaque in the mid-infrared. Therefore, such small reflectance is synonymous with high emissivity, according to Kirchhoff's law and energy conservation principle, which paves the way to efficient radiation sources.

Figure 2(a) & (b) displays the top view SEM images of (a) low-doped sample and (b) highly doped sample and it is observable that the density of darkest spots has increased for the latter sample. Consequently, Figure 2(c) & (d) demonstrates the 3D reconstruction and side view SEM images of 1.3 µm² area of the BSi samples for the two doping levels, all process parameters being identical otherwise. We have chosen a part of the entire sample area to perform the study and establish our conclusions. The chosen sample area for each image has the highest number of dark spots and hence would be ideal to represent the total variation in the brightest and the darkest spots of the image representing the height and periodicity of the BSi samples. One can clearly observe a large increase of the BSi peak's density with the high doping and sharper peaks are observed. This is confirmed and quantified by statistical image processing based on the grey-level analysis shown in Figure 2(e) & (f). The height distribution(H), is obtained from all the elevation data points of each BSi three-dimensional model and the height is measured using the deepest point as reference as illustrated in Fig. 2(e). We also determine the mean spacing(p) histograms of BSi samples (Fig. 2(f)) by averaging the distances between the centre of each hole and its closest neighbours. We see in Fig. 2(e) and (f) that the number of etched holes has multiplied by more than a factor 3, their mean-periodicity has decreased

from 330 nm to 200 nm, and the number of higher structures (above 5 μm) has also increased considerably.

The sample area that is detectable by the spectrometer in the reflectance measurements of BSi was 1 cm^2, which is the size of our samples and thus we can be sure that the detector covers the entire sample area. Though the SEM statistical analysis is generated from a small area of the BSi samples, it aims to represent the morphological details of the entire sample and illustrate one of the plausible reasons behind low reflectance of BSi. According to Kirchhoff's law of thermal radiation [36], spectral emissivity is equal to spectral absorptivity at a given temperature. Consequently, such small reflectance in this specific wavelength enables considering doped BSi as a potential effective and highly emissive infrared source for various kinds of sensing applications based on spectro-photometry.

4. Conclusion

In conclusion, we show, that the considerably high absorptivity of BSi in the visible range [13] can be extended to the spectral range of thermal radiation (up to 15μm) by using highly doped silicon. This striking behavior is ascribed to the high level of doping of the nanostructured surface. The exceptionally high absorptivity levels also translate into high emissivity of doped BSi. Such properties empower considering doped BSi as a hopeful contender for numerous applications, such as radiative cooling, broadband absorbers including bolometers as well as broadband infrared light sources based on black body emission.

References

[1] K. Q. Le, J. Bai, Q. M. Ngo, and P.-Y. Chen, “Fabrication and numerical characterization of infrared metamaterial absorbers for refractometric biosensors,” *Journal of Electronic Materials*, vol. 46, no. 1, pp. 668–676, 2017

[2] Nefzaoui, Elyes, Karl Joulain, Jérémie Drevillon, and Younès Ezzahri. “Radiative thermal rectification using superconducting materials.” *Applied Physics Letters* 104, no. 10 (2014): 103905.

[3] R. Xu and Y.-S. Lin, “Characterizations of reconfigurable infrared meta- material absorbers,” *Optics letters*, vol. 43, no. 19, pp. 4783–4786, 2018.

[4] Steglich, Martin, Dennis Lehr, Stephan Ratzsch, Thomas Käsebier, Frank Schrempel, Ernst-Bernhard Kley, and Andreas Tünnermann. "An ultra-black silicon absorber." *Laser & Photonics Reviews* 8, no. 2 (2014): L13-L17.

[5] Rephaeli, Eden, Aaswath Raman, and Shanhui Fan. "Ultrabroadband photonic structures to achieve high-performance daytime radiative cooling." *Nano letters* 13, no. 4 (2013): 1457-1461.

[6] Kou, Jun-long, Zoila Jurado, Zhen Chen, Shanhui Fan, and Austin J. Minnich. "Daytime radiative cooling using near-black infrared emitters." *Acs Photonics* 4, no. 3 (2017): 626-630.

[7] Ma, Shijun, Shuang Liu, Qinwei Xu, Junwen Xu, Rongguo Lu, Yong Liu, and Zhiyong Zhong. "A theoretical study on the optical properties of black silicon." *AIP Advances* 8, no. 3 (2018): 035010.

[8] Yu, Xin-Yue, Zhen-Hua Lv, Chun-Hao Li, Xiao Han, and Ji-Hong Zhao. "The optical and electrical properties of co-doped black silicon textured by a femtosecond laser and its application to infrared light sensing." *IEEE Sensors Journal* 16, no. 13 (2016): 5227-5231.

[9] Lv, Jian, Ting Zhang, Peng Zhang, Yingchun Zhao, and Shibin Li. "Review application of nanostructured black silicon." *Nanoscale research letters* 13, no. 1 (2018): 110.

[10] Saab, David Abi, Philippe Basset, Matthew J. Pierotti, Matthew L. Trawick, and Dan E. Angelescu. "Static and dynamic aspects of black silicon formation." *Physical review letters* 113, no. 26 (2014): 265502.

[11] Saab, D. Abi, Shermila Mostarshedi, Philippe Basset, Stéphane Protat, Dan Angelescu, and Elodie Richalot. "Effect of black silicon disordered structures distribution on its wideband reduced reflectance." *Materials Research Express* 1, no. 4 (2014): 045045.

[12] Nguyen, K. N, P. Basset, F. Marty, Y. Leprince-Wang, and T. Bourouina. "On the optical and morphological properties of microstructured Black Silicon obtained by cryogenic-enhanced plasma reactive ion etching." *Journal of Applied Physics* 113, no. 19 (2013): 194903.

[13] Sarkar, S., Elsayed, A. A., Nefzaoui, E., Drevillon, J., Basset, P., Marty, F & Liang, Z. (2019, January). NIR and MIR Absorption of Ultra-Black Silicon (UBS). Application to High Emissivity, All-Silicon, Light Source. *In 2019 IEEE 32nd International Conference on Micro Electromechanical Systems (MEMS)* (pp. 860-862). IEEE.

[14] Sarkar, S., Elsayed, A. A., Marty, F., Drévillon, J., Sabry, Y. M., Zhao, J & Nefzaoui, E. (2019, September). Effects of Doping on the Morphology and Infrared Radiative Properties of Black Silicon. *In 2019 25th International Workshop on Thermal Investigations of ICs and Systems (THERMINIC)* (pp. 1-4). IEEE.

[15] Ko, Byoungsu, Dasol Lee, Trevon Badloe, and Junsuk Rho. "Metamaterial-Based Radiative Cooling: Towards Energy-Free All-Day Cooling." *Energies* 12, no. 1 (2019): 89.

[16] Chen, Yu-Bin, and Z. M. Zhang. “Heavily doped silicon complex gratings as wavelength-selective absorbing surfaces.” Journal of Physics D: *Applied Physics* 41, no. 9 (2008): 095406.

[17] Basu, S. & Francoeur, M. Near-field radiative transfer based thermal rectification using doped silicon. *Applied Physics Letters*. 98, 113106 (2011).

[18] Marquier, François, Karl Joulain, J-P. Mulet, Rémi Carminati, J-J. Greffet, and Y. Chen. Coherent spontaneous emission of light by thermal sources. *Physical Review* B 69, no. 15 (2004): 155412.

[19] Law, S., Adams, D. C., Taylor, A. M. & Wasserman, D. Mid-infrared designer metals. *Optics. Express* 20, 12155–12165 (2012).

[20] Cleary, J. W. et al. IR permittivities for silicides and doped silicon. *JOSA* B 27, 730–734 (2010).

[21] Knowles, N. C. (1984). Finite element analysis. *Computer-aided design*, 16(3), 134-140.

[22] Branz, Howard M., Vernon E. Yost, Scott Ward, Kim M. Jones, Bobby To, and Paul Stradins. "Nanostructured black silicon and the optical reflectance of graded-density surfaces." *Applied Physics Letters* 94, no. 23 (2009): 231121.

[23] Hench, John J., and Z. D. E. N. E. K. Strakoš. "The RCWA method-a case study with open questions and perspectives of algebraic computations." *Electronic Transactions on Numerical Analysis* 31 (2008): 331-357.

[24] H. Ansoft, “3-D Electromagnetic simulation software,” Ansoft corp., Pitts- burgh, PA, 2009.

[25] Xiong, Gang, U. Pal, J. G. Serrano, K. B. Ucer, and R. T. Williams. "Photoluminesence and FTIR study of ZnO nanoparticles: the impurity and defect perspective." *physica status solidi* c 3, no. 10 (2006): 3577-3581.

[26] Dunaev, A. Yu, Yu M. Zolotarevskii, S. P. Morozova, V. I. Sapritskii, G. S. Fidanyan, and A. A. Erikova. "Spectrophotometric Instruments Incorporated into get 156–2015, the State Primary Standard of the Unit of Spectral Regular Transmittance, Unit of Spectral Diffuse Reflectance, and Unit of Spectral Specular Reflectance in the Range of Wavelengths from 0.2 to 20.0 μm." *Measurement Techniques* 61, no. 11 (2019): 1045-1051.

[27] Gittleman, J. I., E. K. Sichel, H. W. Lehmann, and R. Widmer. Textured silicon: a selective absorber for solar thermal conversion. *Applied Physics Letters* 35, no. 10 (1979): 742-744.

[28] Craighead, H. G., R. E. Howard, and D. M. Tennant. Textured thin-film Si solar selective absorbers using reactive ion etching. *Applied Physics Letters* 37, no. 7 (1980): 653-655.

[29] Liu, Xiaogang, Paul R. Coxon, Marius Peters, Bram Hoex, Jacqueline M. Cole, and Derek J. Fray. Black silicon: fabrication methods, properties and solar energy applications. *Energy & Environmental Science* 7, no. 10 (2014): 3223-3263.

[30] Schnell, Martin, Ralf Ludemann, and Sebastian Schaefer. Plasma surface texturization for multicrystalline silicon solar cells. *In Conference Record of the Twenty-Eighth IEEE Photovoltaic Specialists Conference-2000* (Cat. No. 00CH37036), pp. 367-370. IEEE, 2000.

[31] Jansen, Henri, Meint de Boer, Rob Legtenberg, and Miko Elwenspoek. The black silicon method: a universal method for determining the parameter setting of a fluorine-based reactive ion etcher in deep silicon trench etching with profile control. *Journal of Micromechanics and Microengineering 5, no. 2 (1995): 115.*

[32] Jansen, Henri, Meint de Boer, Johannes Burger, Rob Legtenberg, and Miko Elwenspoek. The black silicon method II: The effect of mask material and loading on the reactive ion etching of deep silicon trenches. *Microelectronic engineering* 27, no. 1-4 (1995): 475-480.

[33] Stampfl, J., S. Scherer, M. Gruber, and O. Kolednik. Reconstruction of surface topographies by scanning electron microscopy for application in fracture research. *Applied Physics* A 63, no. 4 (1996): 341-346.

[34] Zhu, Fu-Yun, Qi-Qi Wang, Xiao-Sheng Zhang, Wei Hu, Xin Zhao, and Hai-Xia Zhang. 3D nanostructure reconstruction based on the SEM imaging principle, and applications. *Nanotechnology* 25, no. 18 (2014): 185705.

[35] Bose, S. N. (1924). Planck's law and light quantum hypothesis. *Z. phys*, 26(1), 178.

[36] Howell, John R., M. Pinar Menguc, and Robert Siegel. Thermal radiation heat transfer. *CRC press*, 2015.

Acknowledgements

This work was supported by the I-SITE FUTURE Initiative (reference ANR-16-IDEX-0003) in the frame of the project NANO-4-WATER.